We are IntechOpen, the world's leading publisher of Open Access books Built by scientists, for scientists

4,800
Open access books available

122,000
International authors and editors

135M
Downloads

Our authors are among the

154
Countries delivered to

TOP 1%
most cited scientists

12.2%
Contributors from top 500 universities

CLARIVATE ANALYTICS BOOK CITATION INDEX INDEXED

WEB OF SCIENCE™

Selection of our books indexed in the Book Citation Index in Web of Science™ Core Collection (BKCI)

Interested in publishing with us?
Contact book.department@intechopen.com

Numbers displayed above are based on latest data collected.
For more information visit www.intechopen.com

2

Pacemaker Currents in Dopaminergic Neurones of the Mice Olfactory Bulb

Angela Pignatelli, Cristina Gambardella,
Mirta Borin, Alex Fogli Iseppe and Ottorino Belluzzi
Università di Ferrara, Dip. Biologia ed Evoluzione,
Sezione di Fisiologia & Biofisica – Centro di Neuroscienze,
Ferrara
Italy

1. Introduction

In the olfactory bulb (OB) dopaminergic (DA) neurones constitute a fraction of the cells occupying the most external (glomerular) layer (Halász et al.1977). In this region, populated by three types of interneurons, periglomerular (PG) cells, short-axon cells and external tufted (ET) cells (Halász1990) - often collectively referred to as juxtaglomerular cells - an estimated 10% of the neurones in adulthood are positive for tyrosine hydroxylase (TH) (McLean and Shipley1988; Kratskin and Belluzzi2003), the rate limiting enzyme for dopamine synthesis. Dopaminergic neurones in the glomerular layer include PG cells (Gall et al.1987; Kosaka et al.1985) and a fraction of ET cells (Halász1990). Several studies have focused on the role of dopamine in the olfactory bulb, using immunohistochemical (Baker et al.1983; Guthrie et al.1991), behavioral (Doty and Risser1989), and electrophysiological techniques (Nowycky et al.1983; Ennis et al.2001; Davila et al.2003). The more complete description of the functional properties of DA neurons in the OB is probably the paper of Pignatelli (Pignatelli et al.2005), but it was incomplete, as it did not consider the contribution of the inward rectifier currents, a lacuna which is filled in the present work.

A property shared by many DA neurons in the CNS is their capacity to generate rhythmic action potentials even in the absence of synaptic inputs (Grace and Onn1989; Hainsworth et al.1991; Yung et al.1991; Feigenspan et al.1998; Neuhoff et al.2002). In this paper we show for the first time that DA cells in the glomerular layer of the olfactory bulb possess a pacemaker activity, and we provide an explanation for the ionic basis of rhythm generation in these cells.

There is an additional reason to study the functional properties of DA neurones in the OB other than their role in olfaction. The olfactory bulb is one of the rare regions of the mammalian CNS in which new cells, derived from stem cells in the anterior subventricular zone, are also added in adulthood (Gross2000). In the OB, these cells differentiate in interneurones in the granular and glomerular layers. Among these cells there are DA neurones (Betarbet et al.1996; Baker et al.2001), and this has raised a remarkable interest because, for their accessibility, they could provide a convenient source of autologous DA neurons for transplant therapies in neurodegenerative diseases, like Parkinson's disease.

2. Results

2.1 Localisation and general properties of TH-GFP cells

Generation of transgenic mice (TH-GFP/21-31) was described in previous papers (Sawamoto et al.2001; Matsushita et al.2002). The transgene construct contained the 9.0-kb 5'-flanking region of the rat tyrosine hydroxylase (TH) gene, the second intron of the rabbit β-globin gene, cDNA encoding green fluorescent protein (GFP), and polyadenylation signals of the rabbit β-globin and simian virus 40 early genes.

Cells expressing the GFP transgene under the TH promoter (TH-GFP) occurred primarily in the glomerular layer of the main olfactory bulb (Fig. 1A,B). The intraglomerular processes of these cells displayed high levels of TH-GFP expression, and their intertwine delimitates the glomeruli, with the soma of GFP+ cells laying around them.

Recordings with the patch-clamp technique in the whole-cell configuration were obtained from 368 DA cells in the glomerular layer following the procedures described in Pignatelli et al., 2005.

Cell dimensions were rather variable, as shown in Fig. 1C. Previous studies have suggested that there are two populations of DA neurones in the adult OB, based on size or location (Halász1990; Baker et al.1983). In fact, the distribution of the mean cell diameter of GFP+ cells could be best fitted with two Gaussian curves, identifying two subpopulations with average sizes of 5.67 $\pm$ 0.96 µm and 9.48 $\pm$ 2.39 µm (R^2 = 0.991); the same result could be obtained from the analysis of the membrane capacitances, whose frequency distribution could be best fitted by two Gaussians (5.41 ± 1.5 pF and 10.63 ± 3.45 pF, R^2 = 0.975, not shown). However, we found no significant differences in the properties of the two populations.

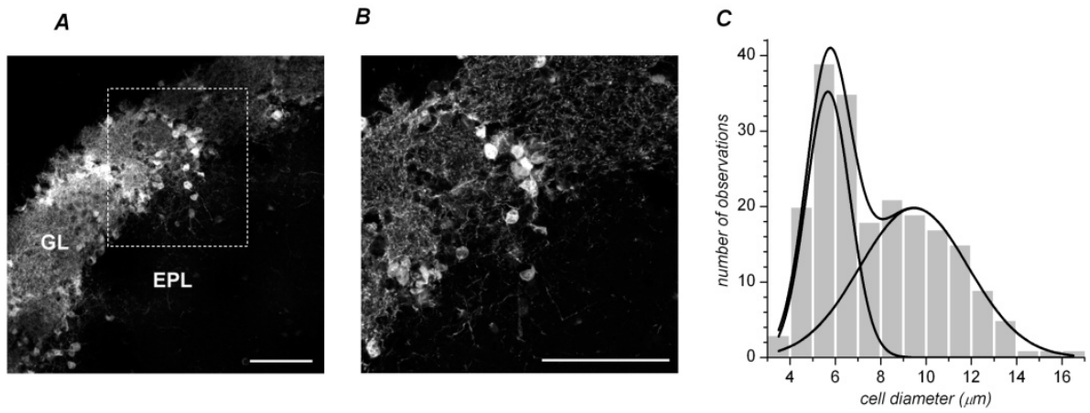

Fig. 1. Morphological properties of TH-GFP cells. A, B - Expression pattern of the TH-GFP transgene in the glomerular layer of the main olfactory bulb in a coronal section. Scale bar 50 µm. C - Frequency distribution of the soma diameter of the cells used in this study. The distribution could be best fitted by two Gaussian curves, identifying two distinct subpopulations of cells.

About 80% of DA neurones were spontaneously active. In the cell-attached configuration, action currents were recorded across the patch, usually structured in a regular, rhythmic pattern (Fig. 2A) with an average frequency of 7.30 $\pm$ 1.35 Hz (n = 31).

After disruption, about 60% of the cells continued to fire spontaneous action potentials under current-clamp condition (Fig. 2B) without any significant alteration of the firing frequency (7.84 ± 2.44 Hz, n = 14). Interspike intervals were rather constant in most of the cells (Fig. 2C), and irregular in others for the presence of sporadic misses. Occasionally, especially in isolated cells (see below), the firing was structured in bursts. We found no correlation of the firing frequency with cell size.

This spontaneous activity was completely blocked by TTX (0.3 μM) or by Cd^{+} (100 μM), but persisted after block of glutamatergic and GABAergic synaptic transmission with kynurenate 1 mM and bicuculline (10 μM), suggesting that it was due to intrinsic properties of the cell membrane and was not driven by external synaptic inputs, as it resulted even more obviously by the observation that spontaneous activity was maintained also in dissociated cells (Fig. 2D).

Occasionally we did observe spontaneous synaptic currents, which were completely blocked by a mixture of 1 mM kynurenate and 10 μM bicuculline (not shown), and which were not further investigated for the purpose of this study.

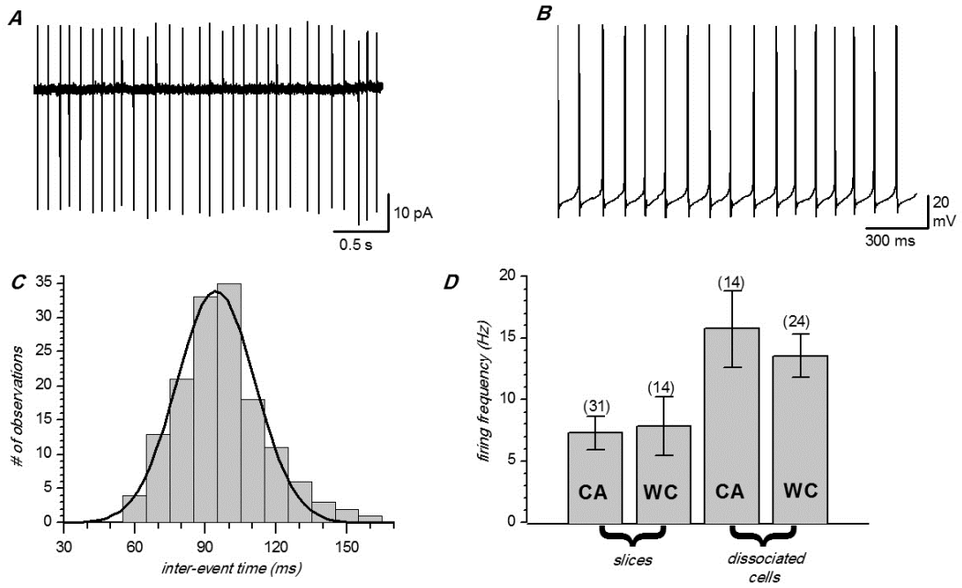

Fig. 2. Spontaneous activity in DA neurones in thin slices. A – Action currents in cell-attached mode B – Action potentials in whole-cell mode C – Frequency distribution of the inter-event time for the cell shown in panel B. D – Frequency of spontaneous firing in TH-GFP cells under the indicated experimental conditions. CA cell attached, WC whole cell.

We studied the dopaminergic neurones under current- and voltage-clamp conditions to characterise the ionic currents underlying spontaneous firing. In voltage-clamped neurones, currents were elicited both by step and ramp depolarisations.

Depolarisation activates a complicated pattern of current flow, in which a variety of conductances coexist, the most prominent of which were a fast transient sodium current and a non-inactivating potassium current (Fig. 3A, B). We identified specific ionic currents present in the cells by measurements of their voltage-dependence and kinetics during step

depolarisations, together with ionic substitution and blocking agents to isolate individual components of the currents. After block of the potassium currents, obtained by adding 20 mM TEA in the perfusing solution and by equimolar substitution of internal K^+ ions with Cs^+, a persistent inward current was observed after the fast transient inward current had completely subsided (Fig 3C, D). The amplitude of this persistent component, measured as the average of the current amplitude during the last 10 ms of the depolarising step, had a maximum amplitude of 223.3 ± 32.2 pA (n=21) at –20 mV, and could be separated in two components, sustained by sodium and calcium ions (see below).

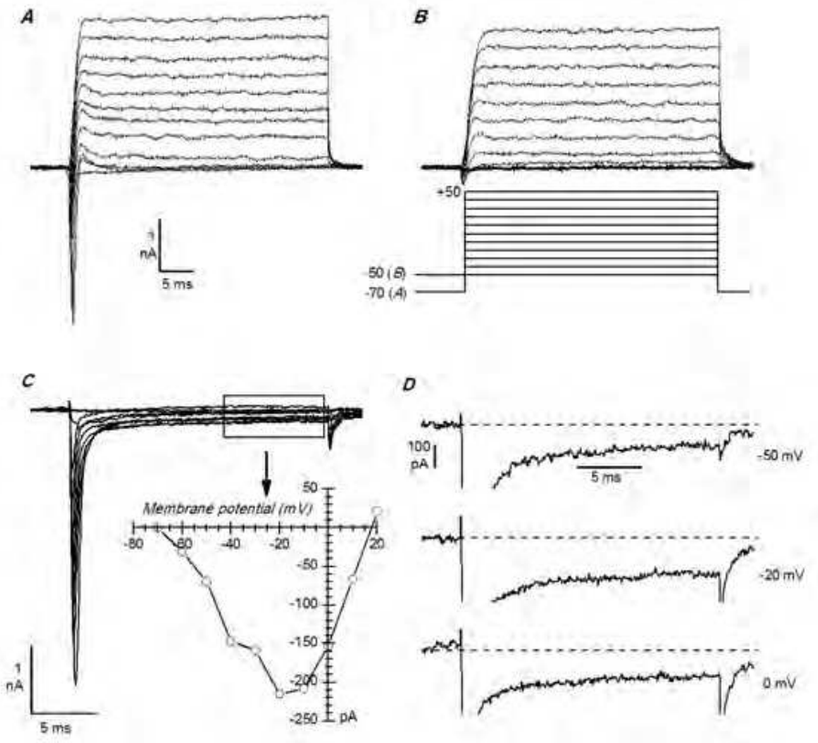

Fig. 3. Responses of DA neurones (PG cells) in thin slices to depolarising voltage steps under different conditions. A, B – Voltage-clamp recordings from the same cell, in normal saline, held at –70 mV (A) and at –50 mV (B), and depolarised to potentials ranging from –50 to +50 mV. C – Inward currents recorded under voltage-clamp conditions in response to depolarising steps ranging from –80 to +50 mV; holding potential was –100 mV. Potassium currents were suppressed by ionic substitution of intracellular K^+ ions with Cs^+, and addition of 20 mM TEA in the extracellular medium. The inset shows the current-voltage relationship of the persistent inward current, averaged at the times indicated by the box. D – Details of some of the traces shown in panel C, at higher magnification, to show the persistent inward current.

2.2 Fast transient Na current

The elimination of the concomitant currents was obtained by blocking the Ca^{2+} current with 100 μM Cd^+, and by equimolar substitution of intracellular K^+ with Cs^+ or NMDG; in addition, the K^+ channels were blocked by adding 20 mM TEA in the perfusing solution

(and occasionally also in the intracellular solution to complete the blockade). Under these conditions, depolarising voltage steps to potentials positive to –60 mV evoked a large, transient inward current, peaking in 0.4 ms at 0 mV which reached its maximum amplitude for steps near –30 mV (Fig. 4A). Its sensitivity to TTX (0.3 μM) at all voltages, and its abolition following removal of sodium ions from the perfusing medium indicate that it is a classical Na-current.

Although it was not always possible to exert an accurate control of membrane potential during the transient sodium current in DA cells in slice preparations (presumably because of currents generated at a distance from the soma on the axon or dendrites), an adequate space clamp and series resistance compensation could be achieved in 7 neurones in which we could obtain a complete series of recordings with and without TTX. The kinetic characterisation of the fast transient Na-current showed in Fig. 4 (and on which is based the numerical reconstruction of this current presented below), was carried out in a homogeneous group of 12 dissociated neurones, averaging 4.5 $\pm$ 0.12 pF, which were electrotonically compact and thus allowed for a more precise space clamp. The results were similar in the two cases, with I/V relationships showing a slightly larger maximum inward current in slices (3784 $\pm$ 369 pA, n=7) than in dissociated cells (3219 $\pm$ 223 pA, n=12), but with the same overall voltage dependence and kinetics.

The peak $I_{Na(F)}$ I-V relationship for a group of twelve dissociated neurones over a range of voltage pulses extending from -80 to +40 mV is shown in Fig. 4B. Reversal potentials for $I_{Na(F)}$ could not be measured directly in our experiments because of uncertainties regarding leakage correction in the presence of large non-specific outward currents. The Na equilibrium potential, evaluated indirectly from the positive limb of the I-V plot (Fig. 4B), is close to +40 mV, about 20 mV more negative than the value predicted by the Nernst equation for a pure Na potential.

The activation process is illustrated in Fig. 4 A-C and G. The fast Na-current develops following a third-order exponential; the activation time constant, τ_m, studied in the –60 to +30 mV range, was computed from the least squares fit of a cubic exponential to the rising phase of the Na-current. In some cases the activation time constant was computed using the method proposed by Bonifazzi et al. (Bonifazzi et al.1988), allowing for the determination of τ_m from the time-to-peak (t_p) and the decay time constant, and consisting in the solution of the equation $t_p = \tau_m \ln(1+n\,\tau_h/\tau_m)$, where n is the order of the activation kinetics. Na-channels activate rapidly, with time constants extending from 0.66 to 0.14 ms in the –60 to +10 mV range. The continuous function describing the dependence of τ_m upon voltage in the range studied, is indicated in the legend of figure 4.

The open channel current as a function of voltage was obtained in a 12 neurones sample from the extrapolation at the time zero of the decaying phase of the current. From the obtained values, the open-channel Na conductance, $g_{Na(F)}$, was calculated using the equation $g_{Na(F)}(V) = I_{Na0}(V)/(V- E_{Na})$, where V is the membrane potential, E_{Na} the sodium equilibrium potential and I_{Na0} is the extrapolation at the zero time of the Na-current.

The conductance-voltage relationship, $g_{Na(F)}(V)$, was described by the Boltzmann equation exhibiting a threshold at about -60 mV, with a slope of 4.34 mV, midpoint at –39.9 mV and a maximum conductance $g_{Na(F)max}$ of 101 nS at –20 mV (Fig. 4C). Finally, the voltage-dependence of the steady-state activation parameter, m_∞, was computed by extracting the

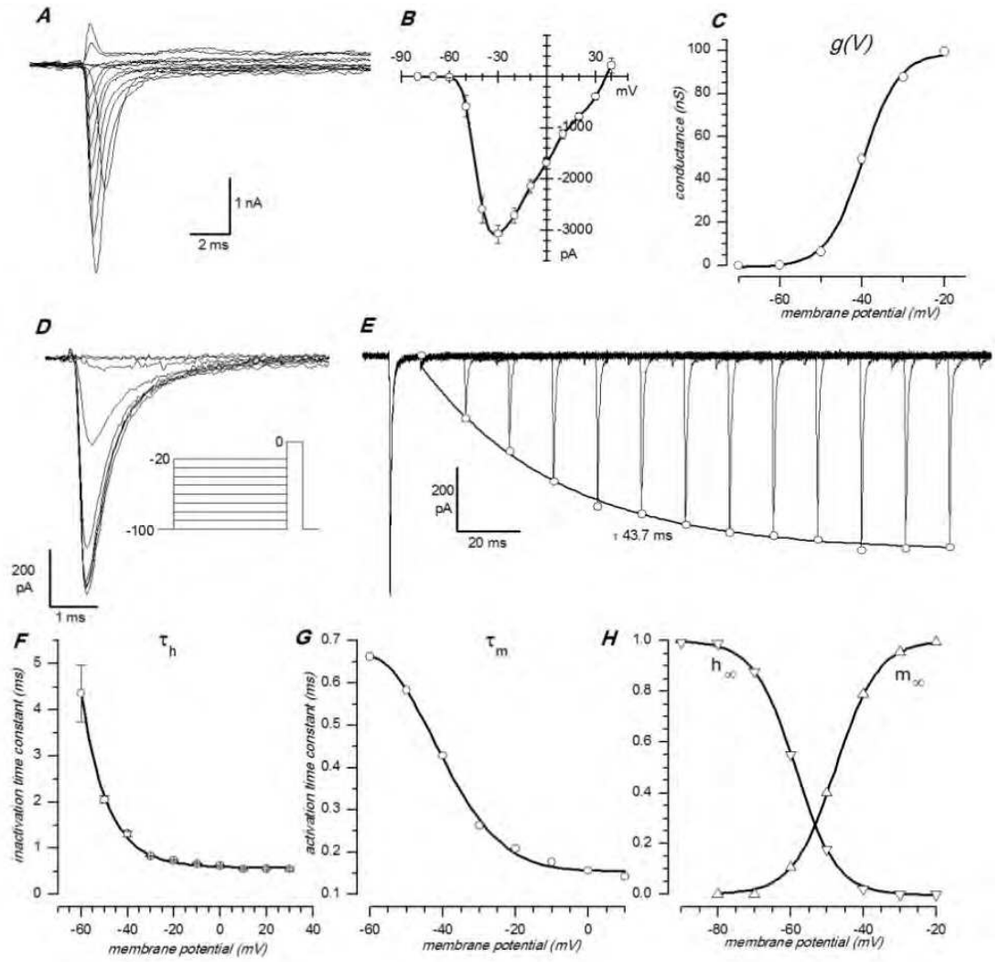

Fig. 4. Properties of fast transient sodium current. A - Family of fast transient sodium current in a TH-GFP cell (PG) in thin slice. Responses to depolarising voltage steps (–90 to + 50 mV) from a holding potential of –100 mV. B – I/V relationship for a group of 12 dissociated cells (average values ± SEM). C – Conductance-voltage relationship for the group of cells shown in B. The continuous curve is drawn according to the Boltzmann equation, with the upper asymptote at 101 nS, midpoint at –39.9 mV and slope of 4,34 mV. D – Development of inactivation. Family of tracings obtained in response to the protocol shown in the inset. E – Time course of removal of inactivation at –80 mV. Family of tracings obtained with a double-pulse protocol, consisting in two subsequent steps to –20 mV, the first from a holding potential of –100 mV, the second after a variable time at –80 mV. F – Voltage-dependence of inactivation time constant, measured from the decay of the current. The continuous curve, describing τ_h in the -60/+30 mV range, obeys the equation: $\tau_h(V) = .58 + .019 * \exp(-V / 11.3)$. G – Voltage-dependence of activation time constant, calculated as explained in the text in a 12 neurone sample. The continuous curve, describing τ_m in the –60/+10 mV range, obeys the equation: $\tau_m(V) = 0.155 + (23.2 / (36.4 * \sqrt{(\pi / 2)})) * \exp(-2*((V+60.62) / 36.4)^2)$ H – Steady-state values of activation and inactivation variables (m and h) of the fast sodium current. The continuous curves obey the equations: $m_\infty(V) = 1/(1+\exp((-47.6-V)/5.8))$, $h_\infty(V) = 1/(1+\exp((V+58.7)/4.5))$.

cubic root from the ratio $g_{Na}(V)$ / $g_{Na(F)max}$ (Fig 4H, upward triangles). The steady-state activation, $m_\infty(V)$, had a midpoint at –47.64 mV and a slope of 5.8 mV.

The steady-state voltage dependence of fast Na inactivation, h_∞, was studied by evaluating the non-inactivated fraction of the Na current as a function of membrane potential (Hodgkin and Huxley1952)(Fig. 4D). The protocol used is illustrated in the inset of the same figure. $I_{Na(F)}$ was measured in each experiment at a constant test voltage of 0 mV after 200 ms preconditioning pulses to various potentials, and plotted after normalisation to the maximum current evoked with hyperpolarisation.

The 200 ms pre-pulse was sufficient to allow the inactivation variable to reach its steady-state value (see Fig. 4E). The steady-state inactivation curve $h_\infty(V)$ thus obtained from a twelve-neurone sample, shows a sigmoidal dependence on voltage which can be fitted by the equation: $h_\infty(V) = (1+\exp[(V-V_h)/k])^{-1}$, where V_h (midpoint) is -58.7 mV and k (slope) is 4.5 mV (Fig. 4H, downward triangles). It should be noted that the inactivating fraction of $I_{Na(F)}$ falls virtually to zero at -30 mV, which is the potential at which $I_{Na(P)}$ reaches its maximum amplitude (Fig. 4B).

Fast sodium channels inactivate rapidly. The decay phase of the current, studied in the –60 to +30 mV range, could be adequately fitted with a single exponential. The continuous function describing the voltage-dependence of inactivation time constant, τ_h, illustrated in Fig. 4F for a ten-neurone sample, can be approximated by the equation indicated in the figure, and has values spanning from 4.4 and 0.6 ms in the voltage range considered.

The rate of recovery from inactivation, was measured using the double-pulse protocol. Na-channel inactivation is removed over a course of a few tens of milliseconds, and the process is markedly voltage-dependent. This is illustrated in Fig. 4E for a typical neurone. The cell was maintained in normal saline at a holding potential of –100 mV, and stepped to –20 mV for 10 ms (τ_h is 0.74 ms at this potential). $I_{Na(F)}$ was then allowed to recover by applying a hyperpolarising pre-pulse of variable duration at different potentials.

Recovery was evaluated by measuring $I_{Na(F)}$ during a second test pulse to -20 mV. In Fig. 4E, a family of $I_{Na(F)}$ currents is shown for the conditioning potential of –80 mV. The current peak as a function of the conditioning pulse duration could be fitted by a simple exponential with a mean value of 42.1 $\pm$ 8.9 ms (n = 14) at –80 mV.

2.3 Delayed rectifier potassium current

A delayed rectifier-type potassium current was present in TH-GFP cells (e.g. Fig. 3B), and it has been kinetically characterised (Fig. 5). The current, isolated by blocking the sodium current with TTX, was calcium-dependent only for a small part (at 0 mV the fraction suppressed by Cd^+ 100 μM was about 10%), and thus it has been modelled as a single component. The equations describing the time- and voltage-dependence of the potassium current are shown in Fig. 5 and detailed in the relative legend.

2.4 Persistent sodium current

In DA cells, after the fast transient Na-current had completely subsided, a persistent inward current showing no sign of inactivation after 200 ms was observed.

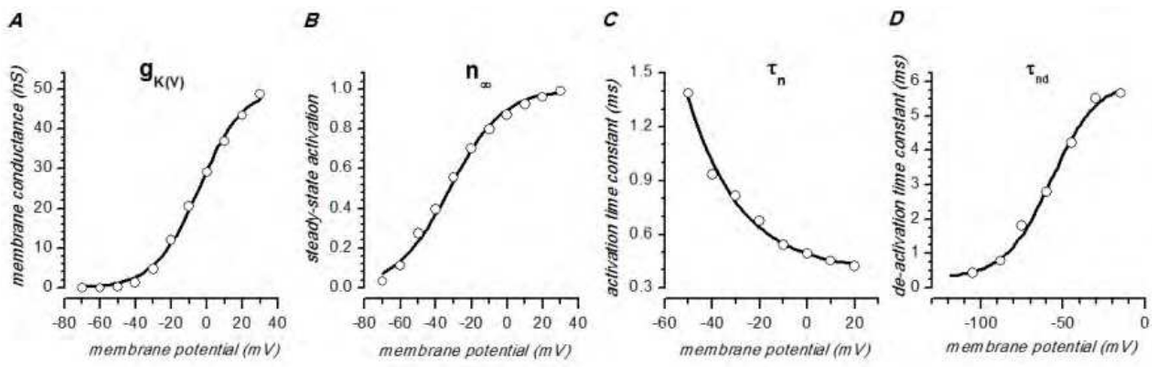

Fig. 5. Properties of delayed rectifier potassium current. A – Conductance-voltage relationship. The continuous curve is drawn according to the Boltzmann equation, with the upper asymptote (maximum conductance) at 50.5 nS, midpoint at –4.1 mV and slope of 12.5 mV. B - Steady-state values of activation (*n*) for the potassium current, obtained from the fourth root of the data shown in *A* after normalisation. The continuous curve obey the equations: $n_\infty(V) = 1/(1+\exp[(-32.2-V)/14.9])$. C - Voltage-dependence of activation time constant (τ_n), obtained by fitting a fourth-order exponential to the rising phase of the current. The continuous curve obeys the equation: $\tau_n(V) = .42 + .097 * \exp(-V / 21.67)$. D – Voltage-dependence of de-activation time constant (τ_{nd}). The continuous curve, describing τ_{nd} in the -105/-15 mV range, obeys the equation: $\tau_{nd} = 6.1 - 5.88/(1+\exp((V+57.6)/14.75))$. This parameter was calculated from the tail currents, independently from τ_n.

We first applied TTX (0.3 to 1.2 μM), which did suppress a significant fraction of the persistent inward current, indicating it received a contribution from a non-inactivating, TTX-sensitive channels. This current-voltage relationship was virtually coincident with the residual persistent current measured after treatment with Cd^{2+} 100 μM (see below), and therefore the data were pooled together. The current-voltage relationship of the fraction of current abolished by TTX or remaining after Cd^{2+} treatment is shown in Fig. 6A.

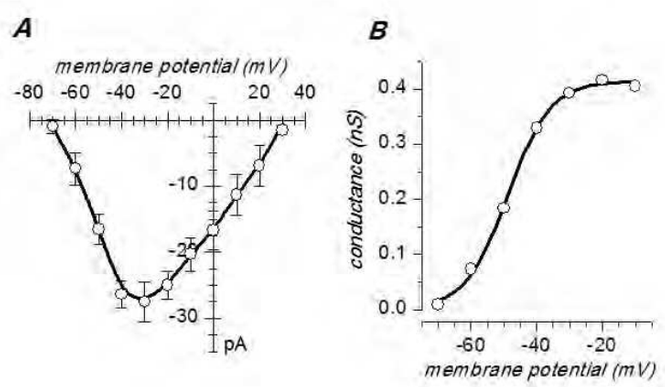

Fig. 6. Properties of persistent sodium current. A – I/V relationship. Pooled data obtained as fraction of non-inactivating current suppressed by TTX (n=12) and residual persistent current after Cd^{2+} block (n=6). B – Conductance-voltage relationship of persistent sodium current, obtained from the average data shown in A. The continuous curve is the Boltzmann fit, with upper asymptote of 0.41 nS, midpoint at –48.8 mV and slope of 6.51 mV.

The persistent sodium current, $I_{Na(P)}$, was activated at potentials more negative than –70 mV, and reached a maximum amplitude of –27.5 ± 2.97 pA at –30 mV. The corresponding conductance-voltage relationship, calculated by dividing the current amplitude by the sodium driving force, could be fitted by a Boltzmann equation with a midpoint at –48.8 mV and a slope of 6.51 mV (Fig 6B). The maximum value of $g_{Na(P)}$ conductance was 0.41 nS, about 200 times smaller than that of the fast sodium current ($I_{Na(F)}$, see below), but contrary to the latter, this current is activated in the pacemaker range, showing an amplitude of –7.3 pA at –60 mV.

2.5 Calcium currents

After block of the TTX-sensitive component and suppression of the K-current by equimolar substitution of intracellular K^+ with Cs^+, a persistent inward current could be observed at the end of prolonged depolarising steps (Fig. 7A, upper trace). This residual fraction could be almost completely blocked by Cd^{2+} or Co^{2+} ions (Fig. 7A, lower traces), suggesting that this second component was sustained by calcium ions. The very small fraction of current remaining after TTX and Cd^{2+} block has not been further investigated in the present study.

Using classical pharmacological tools, ionic substitutions and voltage-clamp protocols, we could dissect the voltage-dependent Ca currents, Ca_v, into several components.

The larger of these components, by its overall kinetics, its voltage-dependence and the absence of inactivation was identified as a possible L-type Ca-current. Its properties were studied in slices, after blockage of the Na-currents with 0.3 – 1.2 µM TTX and of the K-currents by equimolar substitution with Cs^+ in the pipette-filling solution and 20 mM TEA in the perfusing bath. The protocols used were either voltage steps or voltage ramps, giving virtually identical results. The I/V relationship of the Ca-current (Fig 7C), measured in a 10 neurones sample averaging the last 5 ms at the end of a 40 ms depolarising step, had a maximum amplitude of –108.7 ± 11.9 pA at –10 mV. The corresponding conductance-voltage relationship showed a maximum conductance of 2.3 nS, with a midpoint at –25.6 mV.

Equimolar substitution of Ca^{2+} with Ba^{2+} increased by a factor of about 3 the amplitude of this current (Fig. 7C), without changing the I/V relationship or the time constant of activation. On this current we tested the effects of two blockers of L-type calcium channels, nifedipine and calcicludine. The fraction of current blocked by the two drugs at different voltages was quantified by subtraction of I-V data acquired before and after treatment.

The effects of 10 µM nifedipine on peak Ca^{2+} current amplitude was assessed in 6 PG cells (Fig. 7E and F). On average, the drug blocked 61.1 ± 14 % of the current measured at the point of its maximum amplitude (–10 mV).

A 60 aminoacid peptide isolated from the venom of the green mamba (*Dendroaspis augusticeps*), calcicludine (CaC) has been described to have a powerful effect on all type of high-voltage-activated Ca-channels (L-, N-, and P-type) (Schweitz et al.1994). Since one of the regions of the CNS presenting the highest densities of ^{125}I-labeled CaC binding sites is the glomerular layer of the olfactory bulb (Schweitz et al.1994), we tested the ability of this toxin in suppressing the non-inactivating Ca-current found in the DA neurones. CaC (1 µM) was much more effective than nifedipine, with an inhibitory action averaging 72.7 ± 3.13 %.

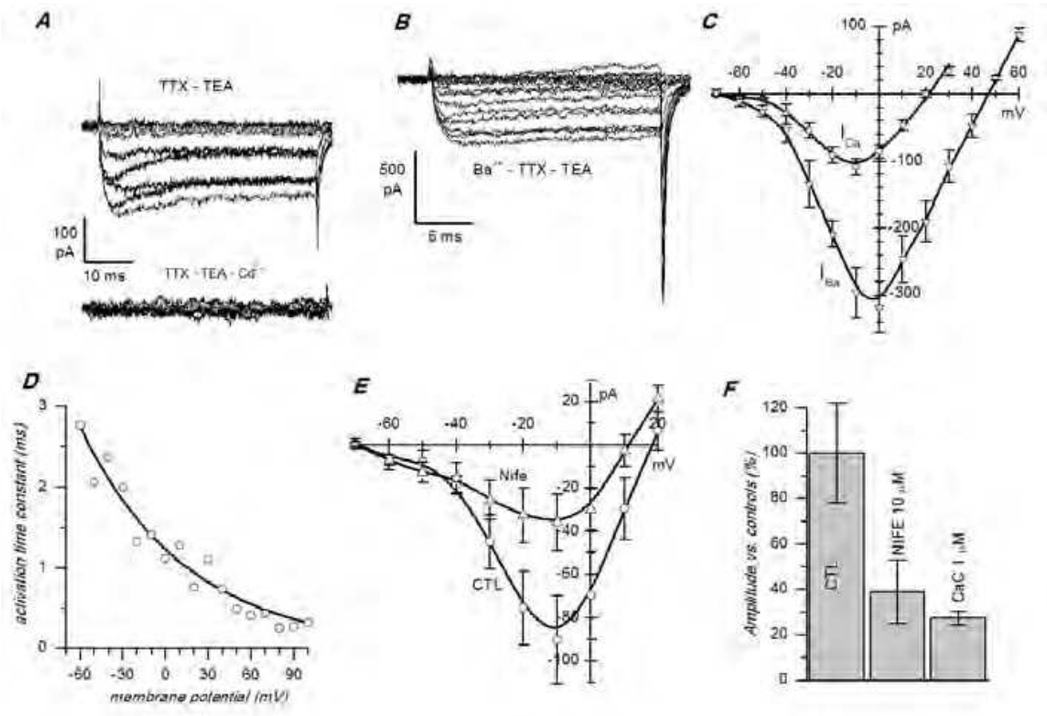

Fig. 7. Properties of HVA calcium currents. A – Calcium current recorded in response to depolarising voltage steps to potentials ranging from –70 to +50 mV from a holding potential of –100 mV. Above: tracings recorded in the presence of 1.2 μM TTX, 20 mM TEA in the extracellular solution, and with Cs^+ as a substitute for K^+ ions in the intracellular solution. Lower tracings were recorded in the same conditions after addition of 100 μM Cd^{2+}. B – Barium currents recorded in the same conditions described for A. C – I/V relationship of Ca and Ba currents in a 10 neurones sample from thin slices. D – Activation time constant, measured in a 10 neurones sample by fitting a single exponential to the rising phase of the current. The continuous line is described by the equation: $\tau_{Ca(L)} = 1.23 + \exp(-V/74.6)$. E – Effect of 10 μM nifedipine on calcium current in a group of six TH-GFP PG cells in slices. F - Histogram showing the effect of nifedipine (10 μM, cells shown in E) and calcicludine (1 μM, not shown, n=7) measured at –10 mV.

We also tried to define if other types of HVA neuronal Ca_v channels (P/Q-, N-) were present in TH-GFP cells. Using classical blockers, like ω-conotoxin GVIA (0.82 μM) that blocks the N-type, or spider toxin ω-agatoxin IVA (10 nM) that blocks P/Q-type channels, we observed the suppression of a fraction of HVA Ca-current remaining after nifedipine block (at –10 mV 38% and 42%, respectively, not shown), suggesting the presence of limited amounts of the corresponding HVA Ca-channels.

Since the long-lasting HVA Ca_v currents were not directly involved in the pacemaker process (see below), and for the dominance of L- over N- and P/Q-type current, for the purpose of the numerical reconstruction of the electrical activity of these cells (see below), they were kinetically modelled as a unique, non inactivating component. The rising phase of the current was fitted by a single exponential, with a time constant of 1.2 + 0.3 ms at 0 mV (n=10, see legend of figure 7D for further details).

Since *in situ* hybridisation experiments have localised the expression of two transcripts (α1G and α1I) of the T-type calcium channel in the glomerular layer of the olfactory bulb (Talley et al.1999; Klugbauer et al.1999), we checked for the presence of LVA Ca-current. Unfortunately several characteristics of these channels hampered their study in our preparation. First, contrary to the cardiac cells or transfected cells, in TH-GFP interneurones this current is small: we have calculated a maximum conductance of 0.35 nS, corresponding to a peak current of about 20 pA at –35 mV. The problem was further complicated by the fact that on one hand it was difficult to get accurate space clamping in slices, and on the other hand, in isolated cell preparations the current was difficult to resolve, probably because of the preferential localisation of these channels on the dendrites (Perez-Reyes2003). Second, the conductance of these channels cannot be significantly increased by substitution of Ca^{2+} with Ba^{2+} ions, as it can be done with HVA channels. Third, there are no effective pharmacological tools for the study of T-type Ca-channels, because they are relatively resistant to most organic calcium channel blockers, such as dihydropyridines, that block the L-type, or peptide toxins, such as ω-conotoxin or ω-agatoxin.

Despite these difficulties, we succeeded in isolating a T-type calcium current in dissociated cells (Fig. 8). The protocol used was a rapid ramp (7 V/s) from –100 to 40 mV, in the presence of TTX (1 μM) and after substitution of Ca^{2+} with Sr^{2+}, which in known to have a slightly higher permeability than Ca^{2+} in T-type Ca-channels (Takahashi et al.1991). Under these conditions, an inward inflection peaking at about –40 mV, distinct from the peak due to the L-type Ca-channels (Fig. 8A), could be seen. Nickel is a nonselective inhibitor of calcium channels, but transient low voltage-activated (LVA) T-type (Perchenet et al.2000; Wolfart and Roeper2002) Ca-channels are particularly sensitive (IC_{50} < 50 μM; (Perez-Reyes et al.1998) whereas other HVA Ca_v channels (L-, P/Q, and N-type) are less sensitive (IC_{50} > 90 μM; (Zhang et al.1993; Randall1998). In fact Nickel did selectively eliminate the first peak, leaving the second unaltered. The difference, averaged in three cells, is shown in figure 8B, and the conductance, calculated assuming a Ca^{2+} equilibrium potential of 45 mV, is illustrated in figure 8C. The current activates at potentials positive to –65 mV and peaks at about –35 mV, with a maximum conductance of 0.35 nS. The point of half activation is –45.3 mV, which is in line with the known values for this current (Perez-Reyes2003).

2.6 h-current

A likely candidate for the pacemaking process was the inward rectifier current (I_h). In a previous work (Pignatelli et al.2005), analysing the excitability profile of DA PG cells, we failed to detect any significant component activated by hyperpolarization (Fig. 9A). It was therefore with some disconcert that we observed that a drug blocking the h-current (ivabradine, 10 μM) did block the spontaneous activity (see below). We then switched to ionic settings known to enhance the amplitude of the h-current, i.e. high $[K^+]_o$, using an external saline where $[K^+]_o$ was 32.5 instead of 2.5 mM. In these conditions, we observed a measurable current activated by hyperpolarization (Fig. 9B), which could be separated in a classical inward rectifier (KIR) and a typical h-current (Fig. 9C). The h-current was suppressed by ivabradina 10 μM, ZD7288 30 μM and Cs^+ 1 mM (Fig. 9D).

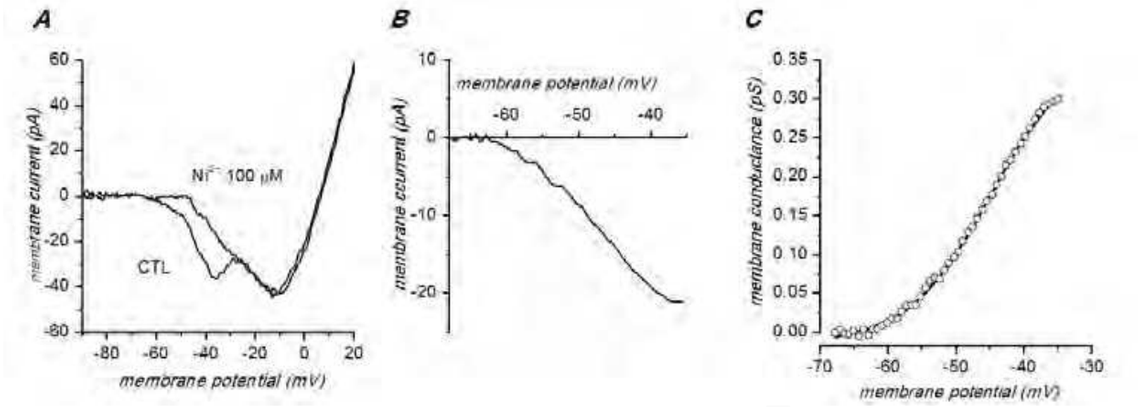

Fig. 8. Properties of the LVA calcium current. A – Voltage-clamp ramps were performed from –80 to +40 mV at a speed of 7 V/s in the presence of TTX (1 µM), and after substitution of Sr^{2+} for Ca^{2+}; the traces were corrected for leakage. Under these conditions, a distinct bump can be seen preceding the HVA calcium current (here peaking at –10 mV), which is selectively suppressed by Ni^{2+} 100 µM. B - Transient Ca-current generated using the protocol described in A calculated by subtracting the current-voltage curves in control and in the presence of 100 µM Ni^{2+}. The low-Ni^{2+} sensitive current (average from three cells) is activated at membrane potentials more positive than –60 mV. C – Conductance-voltage relationship of the low-Ni^{2+} sensitive current. The continuous line is a Boltzmann fit, with a midpoint at –45.3 mV and a maximum conductance of 0.35 nS. All recordings in this figure were performed from spontaneously bursting dissociated TH-GFP cells.

I_h was evoked by a family of seven hyperpolarizing voltage steps (step amplitude -10 mV; step duration 3 s) from the holding potential of -40 to - 130 mV. The steps were applied in 7-s intervals. I_h was calculated as the difference between the membrane current at the end of the voltage step (I_{ss}) and the instantaneous current (I_{inst}) measured after the settling of the capacitative transient. To determine I_h voltage dependence, activation curves were constructed from I_h tail currents, which were calculated by subtracting the pre-step holding current from the peak of the tail current. The activation curves were fitted by the Boltzmann function to estimate the potential of half-activation (V_{50} , -91 mV) and the slope factor (k, 5 mV).

I_h time dependence was studied by fitting current traces (from -100 to -130 mV) with a single exponential function. The activation time constant gave values ranging from 361 ± 112 ms at -100 mV to 155 ± 23 ms at -130 mV (n=10).

The reversal potential, calculated from the reversal of the tail currents (not shown) was -47 mV, from which the maximal conductance could be calculated, giving a value of 1.37 nS.

2.7 KIR current

KIR 2.1 channel subunits are highly expressed in the olfactory bulb, with the higher density in the glomerular layer (Prüss et al.2005), and KIR conductances are found in many dopaminergic systems, as in nucleus accumbens (Perez et al.2006) and substantia nigra (Bausch et al.1995). Here we describe a KIR conductance in the dopaminergic neurones of the olfactory bulb.

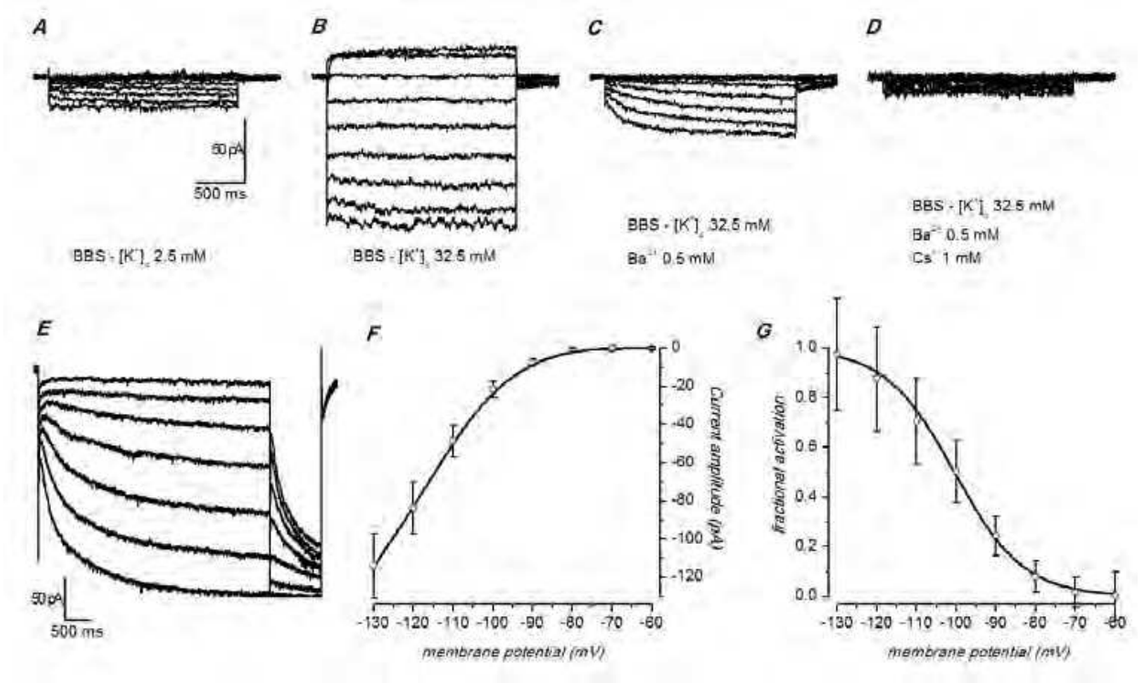

Fig. 9. Properties of the h-current. A,B – Currents activated by hyperpolarizing steps in normal saline and in high K^+, respectively. C – Currents activated by hyperpolarization in high K^+ and after blockage of the KIR component with Ba^{2+} 0.5 mM. D – Same as C after addition of a blocker of the h-current (Cs^+ 1 mM) E – Representative current traces for the analysis of activation. The membrane was held at -40 mV, depolarised to test voltages from -60 to -130 mV in 10 mV increments. I_h tails were elicited in response to a second pulse to −130 mV, following test voltages (see methods for explanation) F – I/V relationship of the h-current for a group of 15 cells. G – Fractional activation of the h-current as a function of voltage.

After block of the h-current with ivabradine 10 μMA, and using high concentration of K^+ in the external saline in order to enhance this KIR-current, a family of almost pure tracings could be evoked by hyperpolarising steps ranging from -50 to -130 mV in 10 mV increments, staring from a holding potential of -40 mV (Fig. 10A); the current could be rapidly and reversibly blocked by Ba^{2+} 0.2 mM (Fig. 10B), and from the I/V curves (Fig. 10C) we calculated a reversal potential of -44 mV (E_K -33 mV), giving conductance of 2 nS at the steady state.

2.8 Spontaneous activity

The presence of autorhythmic activity was the most salient feature of DA cells in the olfactory bulb, so the first efforts were aimed at elucidating the underlying mechanisms. We first tried to understand if the spontaneous activity was due to the presence of pacemaker currents or to synaptic mechanisms reverberating excitation from one cell to the other. Dissociated TH-GFP cells conserved their capacity of generating rhythmic activity, clearly indicating that this is an intrinsic property of these cells. Dissociated TH-GFP cells showed a spontaneous frequency of firing of 13.57 ± 1.79 (n=24) and 15.75 ± 3.12 (n=14) in whole-cell

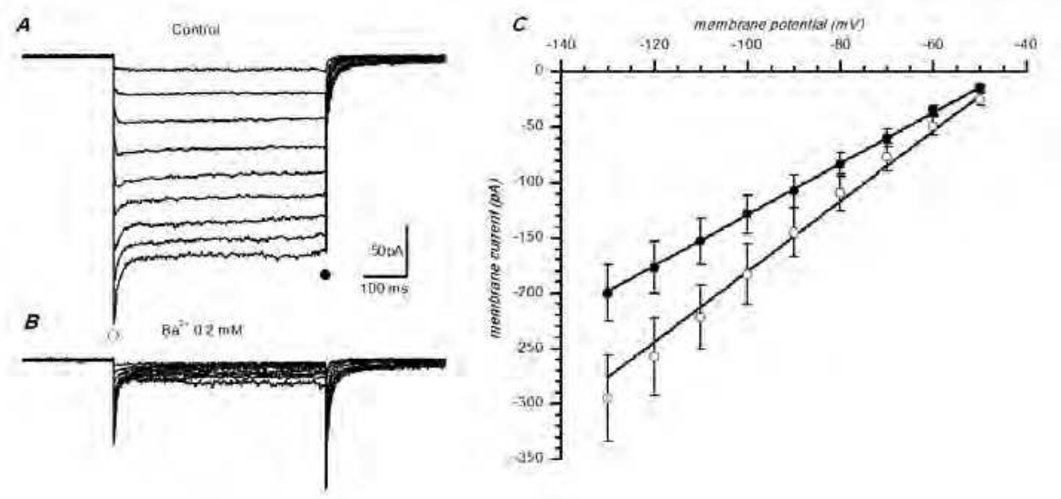

Fig. 10. Properties of the KIR current. A – Family of responses to hyperpolarizing steps from -50 to -130 mV in 10 mV increments from the holding potential of -40 mV. The h-current was blocked by ivabradine 10 μM, and the external saline was modified with high K^+ (32.5 mM) to enhance the KIR amplitude. B – Same as A, but with the addition of Ba^{2+} 0.2 mM. C - I/V relationship of the KIR-current measured at the onset (open circle) and at the steady state (filled circle), at the time points marked in A by the relative symbols; average values ± SE from 11 cells. The reversal potential, calculated from the intercept of the x-axis, was -44 mV, not too far from the E_K, which was -33 mV.

and cell-attached modes respectively (Fig. 2D). This frequency was about double the corresponding value observed in thin slices, suggesting the existence in semi-intact tissue of some inhibitory control, possibly autoinhibition, which has not been further investigated in this study.

2.9 The pacemaker currents

We next tried to elucidate the ionic basis of the pacemaker current underlying the spontaneous firing.

The presence of the h-current, typically associated with the pacemaking process in a large number of autorhythmic cell (see (Wahl-Schott and Biel2009) for a review) has suggested that it could play its archetypal role also in bulbar DA neurons. The I_h blockade with ivabradine did break the spontaneous activity, but this effect was associated to a prominent hyperpolarization (Fig. 11A). It was therefore necessary to clarify if this block was the demonstration of a direct role of the h-current in the pacemaker mechanism, or only a secondary effect, due to the hyperpolarization. If, in the presence of ivabradine block, the membrane was depolarised to the original resting potential, then the spontaneous activity resumed immediately (Fig. 11B), clearly showing that the h-current had no direct role in it.

We next analysed the role of the Ca-current. Ca^{2+} is involved in the pacemaker process, as Cd^{2+} 100 μM completely and reversibly blocked the spontaneous firing (Fig 12B). Then, using a panel of different Ca_v channels inhibitors, we tried to define which types of neuronal Ca_v channels (L-, P/Q-, N-, R-, and T-type) contributed to the pacemaker current.

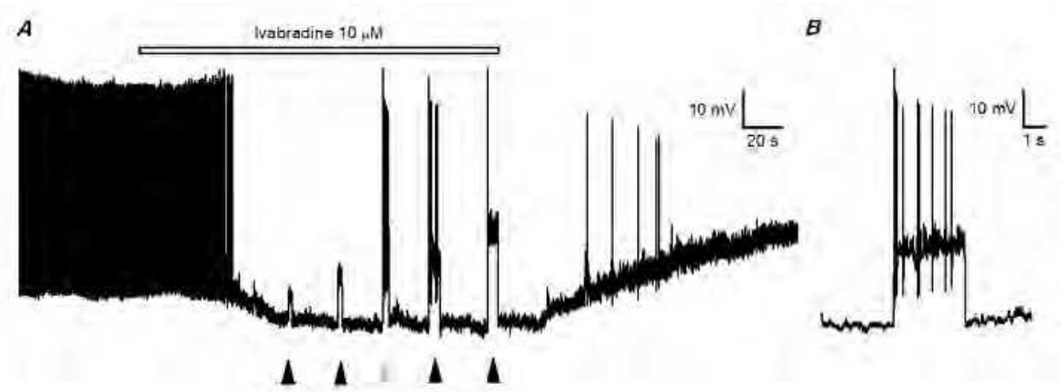

Fig. 11. Effect of blockers of h-channels on spontaneous firing. A – Ivabradine (10 μM, bar) block of spontaneous activity; note the large hyperpolarization. At the times indicated by arrowheads, depolarising currents of increasing amplitudes were delivered. B - Enlargement of the response to the third injection of depolarising current (grey arrowhead) to show that the block of the h-current does not impairs the spontaneous activity, provided that the membrane is brought back to resting values.

The classical selective L-type Ca-channel antagonist nifedipine (10 μM), which blocked the long-lasting Ca-current by about two thirds (Fig. 7E and F), had no effect at all in the spontaneous firing frequency, either in cell-attached mode (Fig. 12C) or in whole-cell configuration, in a total of 6 cells recorded in slices. Also calcicludine (1 μM), a powerful although less selective HVA channel blocker (Schweitz et al.1994), which inhibited the long-lasting Ca-channel component (73%, Fig. 7F), was equally ineffective, even after very long periods of application (Fig. 12E). Analogous results were obtained using other classical blockers of HVA Ca-channels, like ω-conotoxin GVIA (0.82 μM), which blocks the N-type, or spider toxin ω-agatoxin IVA (10 nM) which blocks P/Q-type channels. Both did suppress a fraction of the residual HVA Ca-current after nifedipine block (at –10 mV 38% and 42%, respectively), suggesting the presence of the corresponding types of HVA Ca-channels, but none of them affected the spontaneous firing (not shown).

Among the remaining candidates for a role in pacemaking was the LVA, T-type. Mibefradil, an anti-hypertensive drug, has been reported to inhibit T-type calcium channel current in cerebellar granule cells (Randall and Tsien1997), sensory neurones (Todorovic and Lingle1998) and spinal motor neurones (Viana et al.1997).

We therefore tried this drug, which proved to be considerably powerful in blocking the spontaneous activity of PG DA neurones, both in cell attached (Fig. 13A) and in whole-cell mode (Fig. 13B). Mibefradil (5 to 10 μM) completely and reversibly blocks the spontaneous activity, inducing an evident hyperpolarisation that on average amounted to about 15 mV (Fig. 13B). Nickel 100 μM, that we have shown to be a selective blocker of T-type calcium current in these cells (Fig. 8A), induced a reversible block of spontaneous firing, also accompanied by a hyperpolarisation of 10-15 mV (Fig. 13C), an effect almost superimposable to that observed with mibefradil, further confirming a role of $I_{Ca(T)}$ in the pacemaking process.

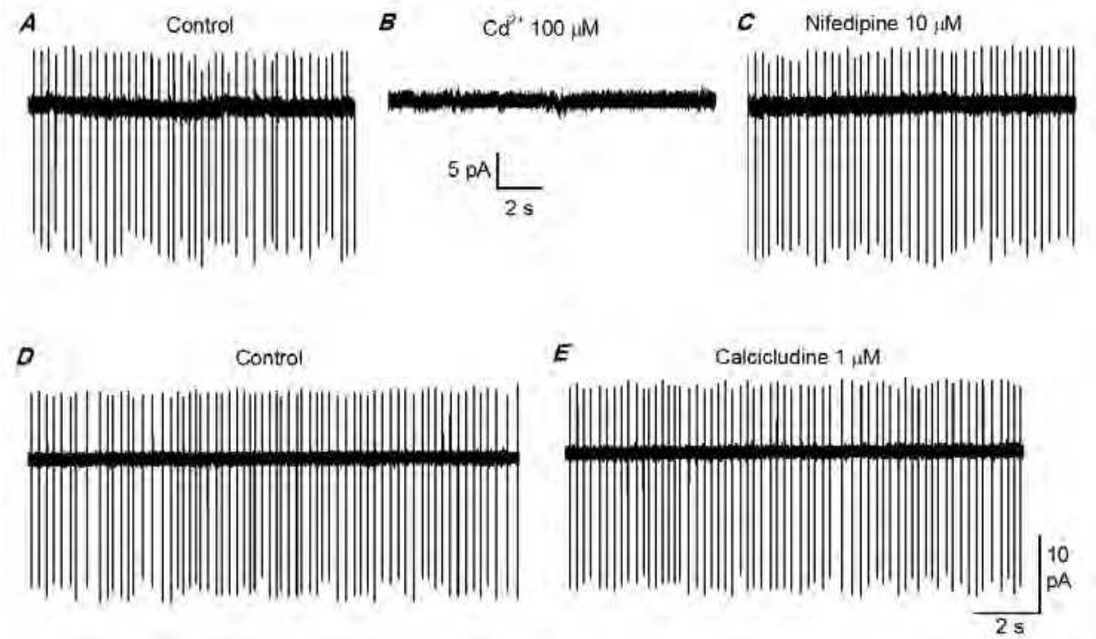

Fig. 12. Effect of blockers of HVA Ca-channels on spontaneous firing. A-B – Effect of the Cd^{2+} (100 μM) on action currents recorded in cell attached mode. C – Effect of L-type Ca-channel antagonist, nifedipine (10 μM). D-E – Effect of L-type Ca-channel antagonist calcicludine (1 μM), recorded 15 min after application.

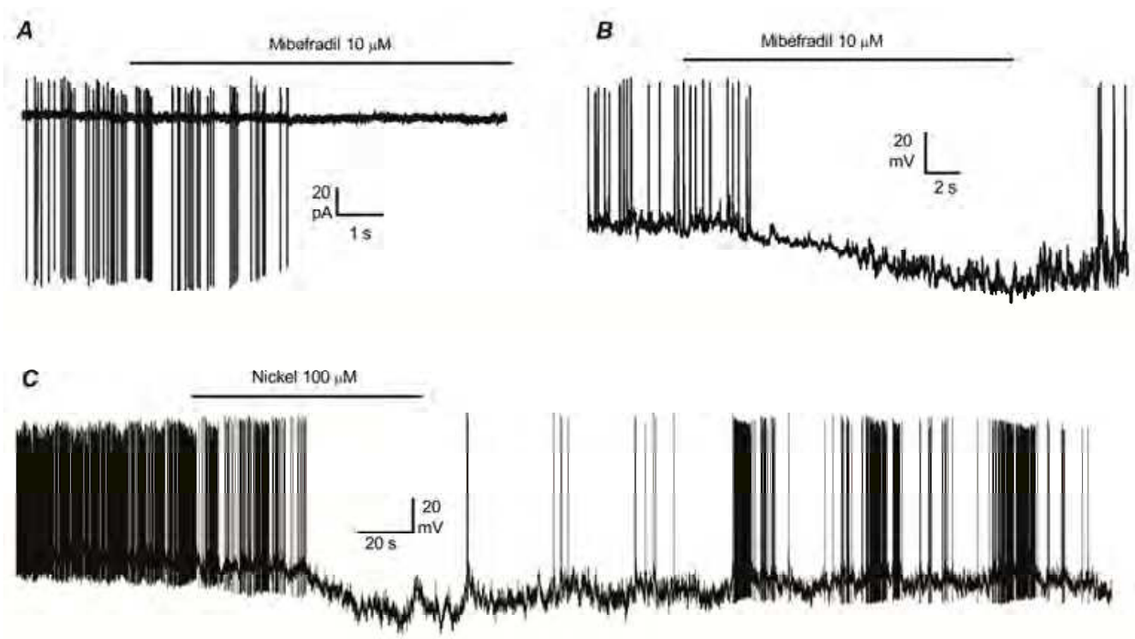

Fig. 13. Effect of blockers of LVA Ca-channels on spontaneous firing. A – Effect of the T-type Ca-channel blocker mibefradil (10 μM) on action currents recorded in cell attached mode. B – Effect of mibefradil in a different TH-GFP cell, recorded in whole-cell configuration. C – Effect of nickel 100 μM on spontaneous firing.

Finally, we investigated the role of the KIR-current on spontaneous activity. The block of the KIR channels with Ba^{2+} 1 mM induced a large depolarization (on average 12 mV), accompanied by a complete stopover of the spontaneous firing.

The effect is illustrated in Fig. 14: a progressive depolarization leads to a complete break of spontaneous activity with a stop at a very depolarised potential (-30 mV in the example shown in figure). In these conditions, the injection of hyperpolarizing currents allows a complete recovery of spontaneous firing, suggesting that the KIR currents plays a relevant role in determining the resting membrane potential, but not in the pacemaking process.

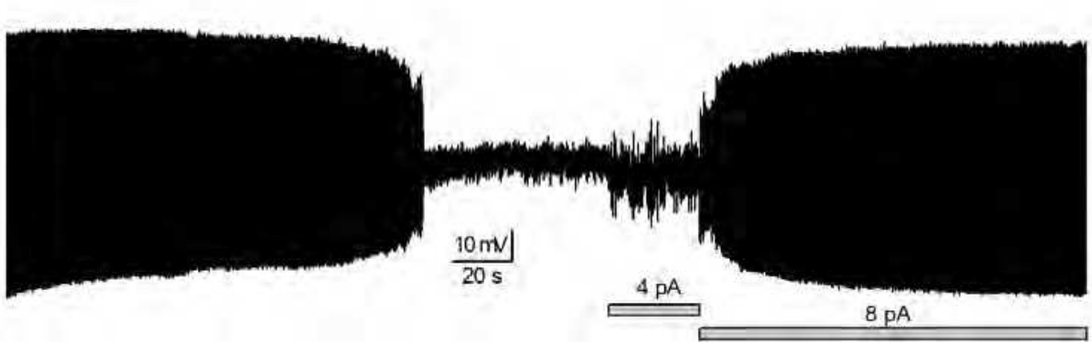

Fig. 14. Effect of blockers of KIR-channels on spontaneous firing. Ba^{2+} (0.5 mM) was applied in the bath 60 s before the beginning of the record; note the progressive depolarization and the stop of any activity in a depolarised state. In this condition, a hyperpolarizing current of 8 pA restores the resting potential, restarting the spontaneous activity.

2.10 Modelling the natural burst firing in bulbar DA neurones

Finally, we have modelled the bulbar DA neurones in Hodgkin-Huxley terms (Hodgkin and Huxley1952), considering the cell as a single electrical and spatial compartment. As for the conductances considered, we incorporated the two sodium currents (fast transient and persistent), the L-type Ca-current, the delayed rectifier K-current, all according to the experimental data presented above, and the T-type calcium current. Since our characterisation of this current was incomplete (and because of the difficulty in obtaining a complete kinetic description of this current), in our model we have integrated our data with others derived from the literature (Wang et al.1996; Perez-Reyes2003), and consistent with our experimental data.

All the equations and parameters used, as well as the assumptions made, are listed in the appendix. The solution of the set of differential equations describing the kinetics of the currents considered lead to the tracings reported in Fig. 15. The model we set up shows intrinsic spiking capabilities with full-size action potentials at the same frequencies observed in TH-GFP cells. The model behaves much like the cells studied: each action potential is followed by a slow depolarisation which brings the model cell at the fast sodium channel threshold, and initiating a new Hodgkin cycle.

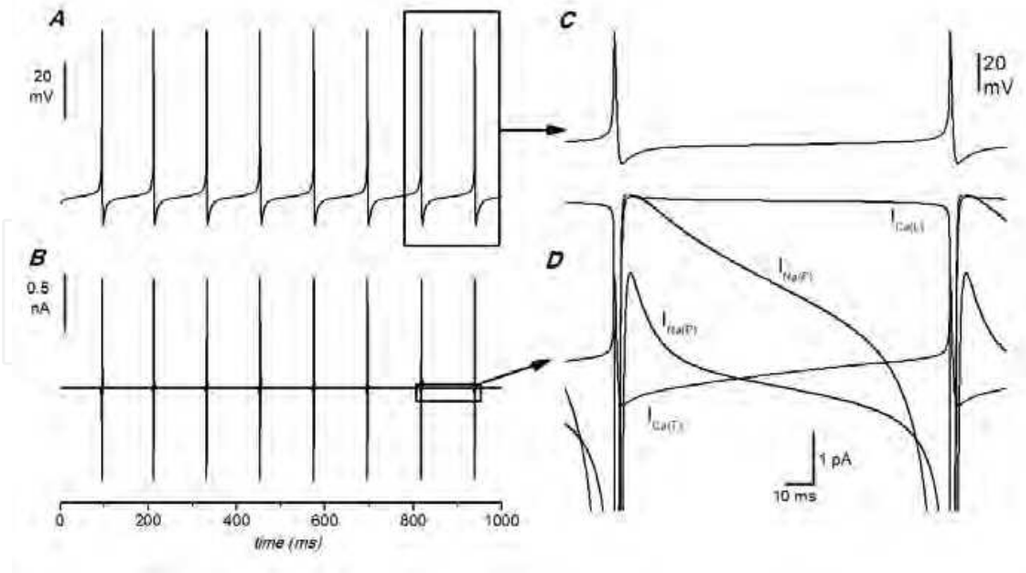

Fig. 15. Numerical reconstitution of spontaneous activity in TH-GFP PG cells. A - Voltage tracings. B - Current tracings including the five conductances: $I_{Na(F)}$, $I_{Na(P)}$, $I_{Ca(T)}$, $I_{Ca(L)}$, $I_{K(V)}$. C, D - Enlargement of the last two events of panels A-B to show the pacemaking process. In D the outward current has been omitted, and the inward currents have been amplified by a factor of about 500 with respect to panel B.

The model is effective to verify the accuracy of the kinetics calculated, and it is particularly useful to understand the details of the interplay of the currents underlying the pacemaking process. The main findings provided by the numerical simulations can be summarised as follows.

First, during the interspike interval, the currents present which cause the progressive depolarisation of the cell are, in order, the T-type calcium current, and then the persistent sodium current. These currents are amazingly small in amplitude (max 4 pA) compared with fast transient sodium and delayed rectifier potassium currents associated to the action potential (about 1 nA), but nevertheless they are sufficient to depolarise these cells, due to their rather high input resistance (about 700 MΩ).

Second, both $I_{Na(P)}$ and $I_{Ca(T)}$ are necessary to sustain spontaneous firing as the selective block of one or both abolish spontaneous activity: the model cell is still capable of responding with a single action potential to the injection of a depolarising current pulse, but it fails to fire repetitively.

Third, the model suggests that it is the T-type calcium current which sets in motion the depolarising process: although essential to the rhythm generation, $I_{Na(P)}$ replaces $I_{Ca(T)}$ only in the second half of the depolarising phase. The T-type calcium conductance amplitude is critical in determining the firing frequency: small changes in its value (from 0.35 to 0.4 nS) are sufficient to drive the intrinsic spiking from 8 Hz to 16 Hz.

Fourth, the HVA calcium currents are unnecessary for the pacemaking process, and their suppression has no consequence on the frequency of spontaneous firing, exactly as in living TH-GFP cells.

Fifth, small changes in the parameters of $I_{Na(F)}$ and of $I_{K(V)}$, such as the half activation point shift of a few millivolts, were sufficient to arrest spontaneous firing but did not affect the capacity to respond with single action potentials to depolarising stimuli. This proves that the pacemaking process is due to an interplay of conductances which are in a delicate and precise equilibrium. Furthermore it confirms the model is capable of capturing the essential features of the excitability profile of these cells.

The model thus confirms that, in addition to $I_{Na(P)}$, another component is necessary to sustain repetitive firing, a T-type calcium current. Together with the experimental finding that treatments which block $I_{Ca(T)}$, such as mibefradil and nickel at micromolar concentrations, are both capable of preventing repetitive firing. Therefore, it appears that such current is an essential component of the pacemaking process.

3. Discussion

This study aims at providing a description as comprehensive as possible of the functional properties of DA neurones in the mammalian olfactory bulb. The animal model used for these experiments, a strain of transgenic mice expressing a reporter protein under the TH promoter (Sawamoto et al.2001; Matsushita et al.2002), allows an easy identification of DA neurones both in thin slices and dissociated cells, proving to be a superb tool for targeting live DA neurones in electrophysiological studies. The main results obtained are the demonstration that DA neurones in the OB are autorhythmic, and the description of the interplay of subthreshold currents underlying intrinsic spiking.

3.1 Distribution and general properties of DA neurones

Neurones expressing high levels of the reporter protein were found in the glomerular layer, as expected from abundant literature, indicating that this is the only region of the main olfactory bulb where TH is expressed (Halász1990; Kratskin and Belluzzi2003). A previous study in the same mice strain has demonstrated an overlapping expression of the fluorescent reporter and TH protein in olfactory bulb only in those DA neurons that received afferent stimulation from receptor cells (Baker et al.2003).

DA neurones in the mice OB have a complement of voltage-dependent currents, which have been kinetically characterised in our study. Among these, the persistent Na current deserves some comment. Many neurones in the mammalian CNS have a non-inactivating component of the TTX-sensitive sodium current (Crill1996). Although its magnitude in bulbar DA neurones is about 0.5 % of the transient sodium current, $I_{Na(P)}$ appears to have an important functional significance because it is activated at potentials 8-10 mV more negative than the transient sodium current. At this potential few voltage-gated channels are activated and the neuron input resistance is high. The conductance-voltage relationship for $g_{Na(P)}$ in TH-GFP DA neurones has a half-activation point at –47.7 mV, very close to the values found in hippocampal CA1 neurones (French et al.1990), and pyramidal neurones of the neocortex (Brown et al.1994). Although this current might appear small, 7.3 pA at –60 mV (Fig. 6A), it suffices to depolarise the cell membrane of these cells, which have an average input resistance of 700 MΩ, by about 5 mV.

We have considered the possibility that $I_{Na(P)}$ is in fact a window current, the steady current predicted by the HH model and arising from overlap of the steady-state activation and

inactivation curves for sodium conductance (Attwell et al.1979; Colatsky1982). Based on the kinetic analysis of the fast Na-current described in the previous paragraph (Fig. 4H), we calculated the window current at different potentials. The numerical simulation indicates this current does provide a measurable contribution to the TTX-sensitive persistent inward current. However, this contribution, which is maximum at –55 mV, becomes virtually zero at –30 mV (Fig. 4H), the potential at which the persistent sodium current displays its maximum amplitude (Fig. 6A). In other words, $I_{Na(P)}$ and the window current of $I_{Na(F)}$ develop at different potentials, and therefore are distinct currents.

3.2 Interaction of ionic currents to produce spontaneous firing

The pharmacological treatments, ion substitution experiments, kinetic analysis and numerical simulations allow a rather precise understanding of mechanisms underlying spontaneous firing in TH-GFP cells. The analysis indicates that the slow depolarisation between spikes results from an interplay between the persistent, tetrodotoxin-sensitive sodium current and the T-type calcium current.

The role of a calcium current in rhythm generation is revealed by the rapid and reversible block of the spontaneous firing by Cd^{2+}, both in slices and in dissociated cells (Fig. 12B). However, among the many HVA Ca-channels present in the DA neurones of the olfactory bulb (a large L-, and smaller N- and P/Q types), none proved to be effective in the control of spontaneous firing. On the contrary, conditions which are known to block the LVA T-type Ca-channels (mibefradil and nickel in the micromolar range) did break off the spontaneous activity.

We developed a numerical HH-type model (Hodgkin and Huxley1952), based on the kinetic characterisation of the voltage-dependent currents described above, which appears to be capable of reproducing fairly well the behaviour of TH-GFP cells. The model was designed in order to verify the accuracy of our kinetic analysis, and, moreover, in order to understand the mechanisms underlying the intrinsic spiking.

Our model reproduces the properties of real neurones, and clearly indicates that the rhythm generation requires the presence of both $I_{Na(P)}$ and $I_{Ca(T)}$: in the absence of any of the two currents, the model can respond with a single action potential to a depolarising pulse, but is unable to produce repetitive firing.

The model shows that the current which sets in motion the spontaneous spiking is the T-type calcium current, which in turn brings into play the persistent sodium current. In spite of the limits inherent to this type of models, we note that small changes in the kinetic parameters lead to the loss of intrinsic spiking but not of the capacity of the cell to respond with a single action potential to the “injection” of a short depolarising current step, thus suggesting that the model has captured the essential features of the real cell.

3.3 The role of hyperpolarization-activated currents

Our results exclude a direct contribution of the h-current to the spontaneous firing and, although less conclusively, also for the KIR current. However, it is of great interest that, as we show, both currents exert a powerful control on the resting membrane potential, the first depolarising, the second hyperpolarising the membrane at rest. The resting membrane

potential, therefore, whose influence on the interplay of pacemaker currents can be well understood with the numerical model proposed, can be adjusted in either directions by a modulation of the two hyperpolarization-activated currents. Both currents can be modulated by a variety of neurotransmitters (see (Biel et al.2009) and (Hibino et al.2010) for recent reviews on h-current and KIR, respectively). Interestingly, some intracellular pathway, like AC/cAMP, can act on both I_h and KIR, enhancing the first and hampering the second (Podda et al.2010); the contrary effect is also observed, e.g. in the rat substantia nigra neurones, where bath application of noradrenaline or dopamine both inhibit I_h and increase the KIR conductance (Cathala and Paupardin-Tritsch1999). Elucidating these interactions will be a critical step in order to understand the functioning of these cells and, in a longer perspective, the still elusive role of dopaminergic neurones in signal processing in the olfactory bulb.

3.4 Significance to olfactory function

Our results, and especially the indication that DA neurones in the glomerular layer are autorhythmic, open the field to many speculations.

It is known that the glomerular neuropile, far from being a homogeneous structure, shows a complex subcompartimental organisation: within a single glomerulus, olfactory nerve (ON) islets delimit areas in which dendritic branches receive sensory input from ON terminals, and are well separated from non-ON zones, from which ON terminals are excluded (Chao et al.1997; Kasowski et al.1999; Toida et al.2000). Some TH-immunoreactive PG cells arborise on the ON islets, others in the non-ON zone (Kosaka et al.1997). Although it has been reported that in some mouse strains TH positive cells are not in contact with ON terminals (Weruaga et al.2000), in the strain used for these experiments – C57BL/6J, one of the most commons - such contacts have been demonstrated (T. Kosaka and K. Kosaka, personal communication).

The glomerular compartmentalisation supports the hypothesis that information processing is subdivided regionally within the mammalian glomerulus (Kasowski et al.1999). DA neurones establishing contacts in ON- or in non-ON zones, possibly play different roles. Within the ON zones, dendrites of DA neurones receive excitatory synapses from ON axon terminals (Chao et al.1997; Kasowski et al.1999; Toida et al.2000). It has been reported that D2 dopaminergic receptors are located in ON terminals (Levey et al.1993; Coronas et al.1997), and electrophysiological studies have shown that their activation can reduce the probability of glutamate release, and hence the excitation of projection neurones (Duchamp-Viret et al.1997; Hsia et al.1999; Berkowicz and Trombley2000; Ennis et al.2001). In fact, the most significant impact of DA neurones is expected at the level of the synaptic triad formed by the ON and the dendrites of mitral/tufted (MT) cells and PG cells (Bardoni et al.1996), where DA neurones directly control the input of projection neurones from receptor cell axons (Brünig et al.1999). Since the ON islets appear to be further segregated from the rest of the glomerular neuropile due to the presence of "glial wraps" (Kasowski et al.1999), the spontaneous activity of DA neurones (which implies continuous release of dopamine within a restricted space), would create a condition of tonic inhibition of the ON.

In addition, DA neurones send their dendrites also in non-ON zones, where they contact dendrites of projection neurones and interneurons, and centrifugal axons. Projection

neurones express D1 and D2 receptors (Brünig et al.1999; Davila et al.2003) , and it has been shown that dopamine exerts a complex modulatory action between them and interneurons (*ibidem*), an effect that also in this case would be amplified by the restricted space of the glomerular neuropile. Within this framework, dopamine might play a central role in the processing of olfactory information by acting at two levels: it would control the input of the sensory signal, and it would modulate the mechanism of GABAergic inhibition (Brünig et al.1999; Davila et al.2003).

It remains to be explained why DA neurones in the glomerular region of the OB are among the very few in the mammalian CNS which are generated also in adulthood. On one end this brings up series of questions concerning the mechanisms controlling their migration and differentiation, and, on the other end, it opens interesting perspectives for the exploitation of the olfactory bulb as a source of undifferentiated DA cells that could be expanded *ex vivo* and used for transplants in neurodegenerative diseases.

4. Acknowledgements

This work was supported by grants from MURST (PRIN 2009) and from Programma Medicina Rigenerativa Regione E.R. – Università, 2007–2009.

5. References

Attwell D, Cohen I, Eisner D, Ohba M, Ojeda C (1979): The steady state TTX-sensitive ("window") sodium current in cardiac Purkinje fibres. *Pflugers Arch* 379:137-142.

Baker H, Kawano T, Margolis FL, Joh TH (1983): Transneuronal regulation of tyrosine hydroxylase expression in olfactory bulb of mouse and rat. *J Neurosci* 3:69-78.

Baker H, Kobayashi K, Okano H, Saino-Saito S (2003): Cortical and striatal expression of tyrosine hydroxylase mRNA in neonatal and adult mice. *Cell Mol Neurobiol* 23:507-518.

Baker H, Liu N, Chun HS, Saino S, Berlin R, Volpe B, *et al* (2001): Phenotypic differentiation during migration of dopaminergic progenitor cells to the olfactory bulb. *J Neurosci* 21:8505-8513.

Bardoni R, Magherini PC, Belluzzi O (1996): Excitatory synapses in the glomerular triad of frog olfactory bulb *in vitro*. *Neuroreport* 7:1851-1855.

Bausch SB, Patterson TA, Ehrengruber MU, Lester HA, Davidson N, Chavkin C (1995): Colocalization of mu opioid receptors with GIRK1 potassium channels in the rat brain: an immunocytochemical study. *Receptors Channels* 3:221-241.

Berkowicz DA, Trombley PQ (2000): Dopaminergic modulation at the olfactory nerve synapse. *Brain Res* 855:90-99.

Betarbet R, Zigova T, Bakay RA, Luskin MB (1996): Dopaminergic and GABAergic interneurons of the olfactory bulb are derived from the neonatal subventricular zone. *Int J Dev Neurosci* 14:921-930.

Biel M, Wahl-Schott C, Michalakis S, Zong X (2009): Hyperpolarization-activated cation channels: from genes to function. *Physiol Rev* 89:847-885.

Bonifazzi C, Belluzzi O, Sacchi O (1988): Kinetic analysis of incomplete current tracings according to the Hodgkin-Huxley model. *J Theor Biol* 130:183-190.

Brown AM, Schwindt PC, Crill WE (1994): Different voltage dependence of transient and persistent Na^+ currents is compatible with modal-gating hypothesis for sodium channels. *J Neurophysiol* 71:2562-2565.

Brünig I, Sommer M, Hatt H, Bormann J (1999): Dopamine receptor subtypes modulate olfactory bulb gamma-aminobutyric acid type A receptors. *Proc Natl Acad Sci USA* 96:2456-2460.

Cathala L, Paupardin-Tritsch D (1999): Effect of catecholamines on the hyperpolarization-activated cationic Ih and the inwardly rectifying potassium I(Kir) currents in the rat substantia nigra pars compacta. *Eur J Neurosci* 11:398-406.

Chao TI, Kasa P, Wolff JR (1997): Distribution of astroglia in glomeruli of the rat main olfactory bulb: exclusion from the sensory subcompartment of neuropil. *J Comp Neurol* 388:191-210.

Colatsky TJ (1982): Mechanisms of action of lidocaine and quinidine on action potential duration in rabbit cardiac Purkinje fibers. An effect on steady state sodium currents? *Circ Res* 50:17-27.

Coronas V, Srivastava LK, Liang JJ, Jourdan F, Moyse E (1997): Identification and localization of dopamine receptor subtypes in rat olfactory mucosa and bulb: a combined in situ hybridization and ligand binding radioautographic approach. *J Chem Neuroanat* 12:243-257.

Crill WE (1996): Persistent sodium current in mammalian central neurons. *Annu Rev Physiol* 58:349-362.

Davila NG, Blakemore LJ, Trombley PQ (2003): Dopamine modulates synaptic transmission between rat olfactory bulb neurons in culture. *J Neurophysiol* 90:395-404.

Doty RL, Risser JM (1989): Influence of the D-2 dopamine receptor agonist quinpirole on the odor detection performance of rats before and after spiperone administration. *Psychopharmacology (Berl)* 98:310-315.

Duchamp-Viret P, Coronas V, Delaleu JC, Moyse E, Duchamp A (1997): Dopaminergic modulation of mitral cell activity in the frog olfactory bulb: A combined radioligand binding electrophysiological study. *Neuroscience* 79:203-216.

Ennis M, Zhou FM, Ciombor KJ, Aroniadou-Anderjaska V, Hayar A, Borrelli E, *et al* (2001): Dopamine D2 receptor-mediated presynaptic inhibition of olfactory nerve terminals. *J Neurophysiol* 86:2986-2997.

Feigenspan A, Gustincich S, Bean BP, Raviola E (1998): Spontaneous activity of solitary dopaminergic cells of the retina. *J Neurosci* 18:6776-6789.

French CR, Sah P, Buckett KJ, Gage PW (1990): A voltage-dependent persistent sodium current in mammalian hippocampal neurons. *J Gen Physiol* 95:1139-1157.

Gall CM, Hendry SH, Seroogy KB, Jones EG, Haycock JW (1987): Evidence for coexistence of GABA and dopamine in neurons of the rat olfactory bulb. *J Comp Neurol* 266:307-318.

Grace AA, Onn SP (1989): Morphology and electrophysiological properties of immunocytochemically identified rat dopamine neurons recorded in vitro. *J Neurosci* 9:3463-3481.

Gross CG (2000): Neurogenesis in the adult brain: death of a dogma. *Nat Rev Neurosci* 1:67-73.

Gustincich S, Feigenspan A, Wu DK, Koopman LJ, Raviola E (1997): Control of dopamine release in the retina: a transgenic approach to neural networks. *Neuron* 18:723-736.

Guthrie KM, Pullara JM, Marshall JF, Leon M (1991): Olfactory deprivation increases dopamine D2 receptor density in the rat olfactory bulb. *Synapse* 8:61-70.

Hainsworth AH, Roper J, Kapoor R, Ashcroft FM (1991): Identification and electrophysiology of isolated pars compacta neurons from guinea-pig substantia nigra. *Neuroscience* 43:81-93.

Halász N (1990): *The vertebrate olfactory system: chemical neuroanatomy, function and development.* Budapest: Académiai Kiadó.

Halász N, Hökfelt T, Ljungdahl A, Johansson O, Goldstein M (1977): Dopamine neurons in the olfactory bulb. *Adv Biochem Psychopharmacol* 16:169-177.

Hibino H, Inanobe A, Furutani K, Murakami S, Findlay I, Kurachi Y (2010): Inwardly rectifying potassium channels: their structure, function, and physiological roles. *Physiol Rev* 90:291-366.

Hodgkin AL, Huxley AF (1952): A quantitative description of membrane currents and its application to conduction and excitation in nerve. *J Physiol (Lond)* 117:500-544.

Hsia AY, Vincent JD, Lledo PM (1999): Dopamine depresses synaptic inputs into the olfactory bulb. *J Neurophysiol* 82:1082-1085.

Kasowski HJ, Kim H, Greer CA (1999): Compartmental organization of the olfactory bulb glomerulus. *J Comp Neurol* 407:261-274.

Klugbauer N, Marais E, Lacinova L, Hofmann F (1999): A T-type calcium channel from mouse brain. *Pflugers Arch* 437:710-715.

Kosaka K, Toida K, Margolis FL, Kosaka T (1997): Chemically defined neuron groups and their subpopulations in the glomerular layer of the rat main olfactory bulb .2. Prominent differences in the intraglomerular dendritic arborization and their relationship to olfactory nerve terminals. *Neuroscience* 76:775-786.

Kosaka T, Hataguchi Y, Hama K, Nagatsu I, Wu JY (1985): Coexistence of immunoreactivities for glutamate decarboxylase and tyrosine hydroxylase in some neurons in the periglomerular region of the rat main olfactory bulb: possible coexistence of gamma-aminobutyric acid (GABA) and dopamine. *Brain Res* 343:166-171.

Kratskin I, Belluzzi O (2003): Anatomy and neurochemistry of the olfactory bulb. In: Doty RL, editor. *Handbook of Olfaction and Gustation*, 2nd ed. New York - Basel: Marcel Dekker, pp 139-164.

Levey AI, Hersch SM, Rye DB, Sunahara RK, Niznik HB, Kitt CA, *et al* (1993): Localization of D1 and D2 dopamine receptors in brain with subtype-specific antibodies. *Proc Natl Acad Sci U S A* 90:8861-8865.

Matsushita N, Okada H, Yasoshima Y, Takahashi K, Kiuchi K, Kobayashi K (2002): Dynamics of tyrosine hydroxylase promoter activity during midbrain dopaminergic neuron development. *J Neurochem* 82:295-304.

McLean JH, Shipley MT (1988): Postmitotic, postmigrational expression of tyrosine hydroxylase in olfactory bulb dopaminergic neurons. *J Neurosci* 8:3658-3669.

Neuhoff H, Neu A, Liss B, Roeper J (2002): I(h) channels contribute to the different functional properties of identified dopaminergic subpopulations in the midbrain. *J Neurosci* 22:1290-1302.

Nowycky MC, Halász N, Shepherd GM (1983): Evoked field potential analysis of dopaminergic mechanisms in the isolated turtle olfactory bulb. *Neuroscience* 8:717-722.

Perchenet L, Benardeau A, Ertel EA (2000): Pharmacological properties of Ca(V)3.2, a low voltage-activated Ca^{2+} channel cloned from human heart. *Naunyn Schmiedebergs Arch Pharmacol* 361:590-599.

Perez MF, White FJ, Hu XT (2006): Dopamine D(2) receptor modulation of K(+) channel activity regulates excitability of nucleus accumbens neurons at different membrane potentials. *J Neurophysiol* 96:2217-2228.

Perez-Reyes E (2003): Molecular physiology of low-voltage-activated t-type calcium channels. *Physiol Rev* 83:117-161.

Perez-Reyes E, Cribbs LL, Daud A, Lacerda AE, Barclay J, Williamson MP, *et al* (1998): Molecular characterization of a neuronal low-voltage-activated T-type calcium channel. *Nature* 391:896-900.

Pignatelli A, Kobayashi K, Okano H, Belluzzi O (2005): Functional properties of dopaminergic neurones in the mouse olfactory bulb. *J Physiol* 564:501-514.

Podda MV, Riccardi E, D'Ascenzo M, Azzena GB, Grassi C (2010): Dopamine D1-like receptor activation depolarizes medium spiny neurons of the mouse nucleus accumbens by inhibiting inwardly rectifying K^+ currents through a cAMP-dependent protein kinase A-independent mechanism. *Neuroscience* 167:678-690.

Prüss H, Derst C, Lommel R, Veh RW (2005): Differential distribution of individual subunits of strongly inwardly rectifying potassium channels (Kir2 family) in rat brain. *Brain Res Mol Brain Res* 139:63-79.

Randall AD (1998): The molecular basis of voltage-gated Ca^{2+} channel diversity: is it time for T? *J Membr Biol* 161:207-213.

Randall AD, Tsien RW (1997): Contrasting biophysical and pharmacological properties of T-type and R-type calcium channels. *Neuropharmacology* 36:879-893.

Sawamoto K, Nakao N, Kobayashi K, Matsushita N, Takahashi H, Kakishita K, *et al* (2001): Visualization, direct isolation, and transplantation of midbrain dopaminergic neurons. *Proc Natl Acad Sci U S A* 98:6423-6428.

Schweitz H, Heurteaux C, Bois P, Moinier D, Romey G, Lazdunski M (1994): Calcicludine, a venom peptide of the Kunitz-type protease inhibitor family, is a potent blocker of high-threshold Ca^{2+} channels with a high affinity for L-type channels in cerebellar granule neurons. *Proc Natl Acad Sci U S A* 91:878-882.

Takahashi K, Ueno S, Akaike N (1991): Kinetic properties of T-type Ca^{2+} currents in isolated rat hippocampal CA1 pyramidal neurons, 65 ed, pp 148-155.

Talley EM, Cribbs LL, Lee JH, Daud A, Perez-Reyes E, Bayliss DA (1999): Differential distribution of three members of a gene family encoding low voltage-activated (T-type) calcium channels. *J Neurosci* 19:1895-1911.

Todorovic SM, Lingle CJ (1998): Pharmacological properties of T-type Ca^{2+} current in adult rat sensory neurons: effects of anticonvulsant and anesthetic agents. *J Neurophysiol* 79:240-252.

Toida K, Kosaka K, Aika Y, Kosaka T (2000): Chemically defined neuron groups and their subpopulations in the glomerular layer of the rat main olfactory bulb. IV. Intraglomerular synapses of tyrosine hydroxylase-immunoreactive neurons. *Neuroscience* 101:11-17.

Viana F, Van den BL, Missiaen L, Vandenberghe W, Droogmans G, Nilius B, *et al* (1997): Mibefradil (Ro 40-5967) blocks multiple types of voltage-gated calcium channels in cultured rat spinal motoneurones. *Cell Calcium* 22:299-311.

Wahl-Schott C, Biel M (2009): HCN channels: structure, cellular regulation and physiological function. *Cell Mol Life Sci* 66:470-494.

Wang X, Mckenzie JS, Kemm RE (1996): Whole cell calcium currents in acutely isolated olfactory bulb output neurons of the rat. *J Neurophysiol* 75:1138-1151.

Weruaga E, Brinon JG, Porteros A, Arevalo R, Aijon J, Alonso JR (2000): Expression of neuronal nitric oxide synthase/NADPH-diaphorase during olfactory deafferentation and regeneration. *Eur J Neurosci* 12:1177-1193.

Wolfart J, Roeper J (2002): Selective coupling of T-type calcium channels to SK potassium channels prevents intrinsic bursting in dopaminergic midbrain neurons. *J Neurosci* 22:3404-3413.

Yung WH, Hausser MA, Jack JJ (1991): Electrophysiology of dopaminergic and non-dopaminergic neurones of the guinea-pig substantia nigra pars compacta in vitro. *J Physiol* 436:643-667.

Zhang JF, Randall AD, Ellinor PT, Horne WA, Sather WA, Tanabe T, *et al* (1993): Distinctive pharmacology and kinetics of cloned neuronal Ca^{2+} channels and their possible counterparts in mammalian CNS neurons. *Neuropharmacology* 32:1075-1088.

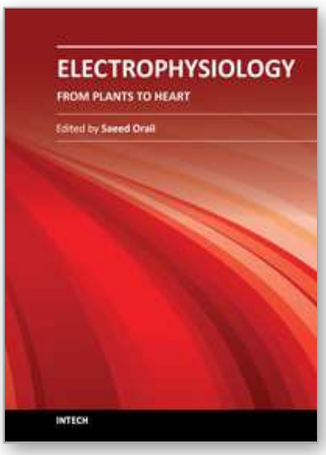

Electrophysiology - From Plants to Heart

Edited by Dr. Saeed Oraii

ISBN 978-953-51-0006-5
Hard cover, 202 pages
Publisher InTech
Published online 03, February, 2012
Published in print edition February, 2012

The outstanding evolution of recording techniques paved the way for better understanding of electrophysiological phenomena within the human organs, including the cardiovascular, ophthalmologic and neural systems. In the field of cardiac electrophysiology, the development of more and more sophisticated recording and mapping techniques made it possible to elucidate the mechanism of various cardiac arrhythmias. This has even led to the evolution of techniques to ablate and cure most complex cardiac arrhythmias. Nevertheless, there is still a long way ahead and this book can be considered a valuable addition to the current knowledge in subjects related to bioelectricity from plants to the human heart.

How to reference

In order to correctly reference this scholarly work, feel free to copy and paste the following:

Angela Pignatelli, Cristina Gambardella, Mirta Borin, Alex Fogli Iseppe and Ottorino Belluzzi (2012). Pacemaker Currents in Dopaminergic Neurones of the Mice Olfactory Bulb, Electrophysiology - From Plants to Heart, Dr. Saeed Oraii (Ed.), ISBN: 978-953-51-0006-5, InTech, Available from: http://www.intechopen.com/books/electrophysiology-from-plants-to-heart/pacemaker-currents-in-dopaminergic-neurons-of-the-mice-olfactory-bulb

INTECH
open science | open minds

InTech Europe
University Campus STeP Ri
Slavka Krautzeka 83/A
51000 Rijeka, Croatia
Phone: +385 (51) 770 447
Fax: +385 (51) 686 166
www.intechopen.com

InTech China
Unit 405, Office Block, Hotel Equatorial Shanghai
No.65, Yan An Road (West), Shanghai, 200040, China
中国上海市延安西路65号上海国际贵都大饭店办公楼405单元
Phone: +86-21-62489820
Fax: +86-21-62489821

IntechOpen